RSC Advances

PAPER

View Article Online
View Journal | View Issue

Cite this: *RSC Adv.*, 2021, **11**, 21073

Application of the synergistic flame retardant europium hydrotalcite/graphene oxide hybrid material and zinc borate to thermoplastic polyurethane

Yi Qian,*[a] Jinying Zheng,[b] Long Li,*[b] Peng Qiao,[a] Ying Li,[b] Yinghui Duan[a] and Guozhang Chang[c]

In this paper, a certain amount of rare earth (europium) was doped into magnesium aluminum salt solution and assembled with graphene oxide (GO) by electrostatic interaction under alkaline conditions. Then, the EuMgAl-LDH/GO hybrid material was synthesized by a hydrothermal method. Its microstructure was analyzed and tested by X-ray diffraction (XRD), energy dispersive spectrometry (EDS), transmission electron microscopy (TEM) and Fourier transform infrared spectroscopy (FTIR), the results indicated that the EuMgAl-LDH/GO hybrid material had been successfully prepared. Next, it was mixed with zinc borate and added to a thermoplastic polyurethane (TPU) (thermoplastic polyurethane) matrix by melting blending. The flame retardant and smoke suppression effect of the composite was tested by conical calorimetry. The results showed that, compared with simple TPU, the PHRR (peak heat release rate), THR (total heat release), PSPR (peak smoke production rate) and TSP (total smoke production) value of the composite material decreased by 65.6%, 16.2%, 61% and 37.1%, respectively. Finally, through analysis of the carbon residue after combustion of the TPU composite material, we found that the formed carbon layer is denser and the char yield is greatly improved.

Received 3rd March 2021
Accepted 10th May 2021

DOI: 10.1039/d1ra01689j

rsc.li/rsc-advances

1. Introduction

Polymer materials are closely related to our life. Take thermoplastic polyurethane (TPU) as an example, it has been widely used in various engineering practices due to its excellent mechanical properties. Unfortunately, most of these materials have poor fire safety and they will produce a good deal of harmful smoke during the burning process, which greatly threatens the safety of people's lives and properties.[1,2] Therefore, various nano additives are added to polymers to improve their flame retardancy. With the strengthening of environmental protection policies, organic flame retardants have gradually been reduced or even partially banned.[3] In recent years, a variety of inorganic flame retardants have been used to improve the flame retardancy of TPU due to their advantages of environmental protection and low cost, among which layered double hydroxides (LDHs) are a typical representative.[4]

However, when conventional hydrotalcite is used as a flame retardant, the amount of addition is often large, which reduces the mechanical properties of the composite and limits its application. Therefore, modified hydrotalcite has been widely studied in recent years.[5] Gao and his coauthors[6] discussed the effects of metal elements, interlayer ions and interlayer distance of LDHs on flame retardant and smoke suppression performance of composite materials. The results show that the metal elements and intercalation ions can play the roles of flame retardant and smoke suppression through catalytic carbonization and dilution of combustible gas. Similar to LDHs, layered rare earth hydroxide is a new layered metal hydroxide material. Wen *et al.*[7] introduced La^{3+} into Zn/Al–CO_3^{2-} LDH, and then added it into the polyvinyl chloride (PVC) resin as a thermal stabilizer. The results showed that ZnAlLa-LDH can obvious enhance the thermal stability of PVC.

As another new two-dimensional layered material, graphene oxide (GO), has become a hot research topic in recent years.[8,9] Because of its unique physical properties, GO has a fine application prospect in the field of flame retardants. Wang *et al.*[10] successfully synthesized the hybrid material that consist of positively charged MgAl-LDHs nanosheet and negatively charged GO nanosheet by means of electrostatic self-assembly, and studied its CO_2 adsorption capacity. Ahmed *et al.*[11] prepared CuAl-LDHS and CoAl-LDHS catalysts with GO nanosheet as the carrier, and found that both materials could catalyze the Ullmann coupling reaction between aryl and cycloalkyl

[a]College of Chemical Engineering, Qingdao University of Science and Technology, Qingdao 266042, China. E-mail: qianyi1962@126.com; lli@yic.ac.cn
[b]College of Environment and Safety Engineering, Qingdao University of Science and Technology, Qingdao 266042, China
[c]State Key Laboratory of High-Efficiency Utilization of Coal and Green Chemical Engineering, Ningxia University, Yinchuan 750021, China

under alkali-free conditions, and shorten reaction time as all as improved the yield. Hong *et al.*[12] prepared hybrid materials of LDH and RGO (reduced graphene oxide)by coprecipitate method, and add it to the PMMA (methyl propylene acid methyl ester), the results show that compare with single LDH and RGO, the hybrid materials can better improve the thermal stability of the composite, reduce the heat and smoke parameters in the test.

Boron family compounds are one of the earliest inorganic flame retardants and are often used as synergy flame retardants. When used in combination with other flame retardants, they can significantly reduced smoke density of the composite.[13,14] Yildiz[15] *et al.* added zinc borate (ZB) to polyurethane (PU) to prepare PU composite sheets. When the addition amount of ZB was only 0.5 wt%, the combustion time of composite films increased by 160% compared with pure PU, and the flame retardant performance was improved. Yang *et al.*[16] mixed ZB with liquid polysiloxane (PSI) to study flame retardant performance of polycarbonate (PC). The experimental results showed that the synergistic effect between PSI and ZB is achieved by cross-linking reaction and the existence of B–O–SI structure reduces the occurrence of melting dripping phenomenon. At the same time, element B can be dragged to the surface of the carbon layer in the form of siloxane of PI, and then together with element Si promote the formation of a tight carbon layer. Compared with pure PSI or ZB system, the system of mixing PSI with ZB obviously improve the flame retardant performance. In addition, ZB has a good flame retardant synergistic effect with magnesium hydroxide, aluminum hydroxide and antimony trioxide.[17]

At present, the research on the flame retardant properties of rare earth hydrotalcite is mainly focused on La-LDHs. In this paper, a new rare earth element europium (Eu) was introduced into the interlayer of hydrotalcite and adopted hydrothermal method to synthesis Eu-LDHs. Then, the rare earth hydrotalcite nanosheets and GO nanosheets were assembled by electrostatic self-assembly to form the Eu-LDH/GO hybrid material. Next, the hybrid material was mixed with zinc borate in a certain proportion and added into TPU by melting blending method to prepare TPU composite material. The flame retardant and smoke suppression of TPU composite was tested by conical calorimeter (CCT), the thermal stability of TPU composites was analyzed by thermogravimetric analyzer (TGA). Finally, the carbon layer after combustion is analyzed to reveal its flame retarding mechanism (Fig. 1).

2. Experimental

2.1 Materials

Zinc borate ($2ZnO\cdot 3B_2O_3\cdot 3.5H_2O$, AR) was purchased Tianjin Damao Chemical Reagent Co. Sulfuric acid (H_2SO_4, 98% aq.), hydrogen peroxide (H_2O_2, 30% aq.), nitric acid (HNO_3, 68% aq.), graphite powder (C, CP), potassium permanganate ($KMnO_4$, AR), aluminum nitrate ($Al(NO_3)_3\cdot 9H_2O$, AR), magnesium nitrate ($Mg(NO_3)_2\cdot 6H_2O$, AR) and sodium hydroxide (NaOH, AR) were all purchased from Sinopharm Chemical Reagent Co. Ltd. (China). Eu_2O_3 was bought from Shanghai Aladdin Chemistry Co. Ltd, China. Thermoplastic polyurethane (TPU, 9380A) was purchased from Germany's bayer, the molecular weight distribution (2000–7000).

2.2 Synthesis of Eu-LDHs

Eu-LDHs was synthesized by coprecipitation and hydrothermal method. First, Eu_2O_3 was dissolved in hot dilute nitric acid to prepare $Eu(NO_3)_3$. The $Eu(NO_3)_3$ solution was configured to a certain concentration and place it in a volumetric flask for use. Then, take a some amount of $Mg(NO_3)_2\cdot 6H_2O$, $Al(NO_3)_3\cdot 9H_2O$ and $Eu(NO_3)_3$ to preparate a solution, make M^{2+}/M^{3+} molar ratio was 2 (keep its ratio unchanged), and gradually change the Eu^{3+}/Al^{3+} molar ratio to 0.01, 0.02, 0.05, 0.1. We transferred the above solution to a three-port flask. After that, the pH of solution was adjusted to 10–11 by adding sodium hydroxide (1 mol L^{-1}) dropwise. The mixture was stirred intensely at 80 °C for 30 min. Then pour it into a Teflon reactor and heat it at 130 °C for 12 h. Finally, the product was washed with deionized water to pH = 7 and dried at 60 °C for 24 h.

2.3 Synthesis of Eu-LDHs/GO hybrid

GO was synthesized from graphite powder by using the Hummers method.[18] Add 60 mL of the mixed solution containing 0.03 mol $Mg(NO_3)_2$ and a certain amount of $Al(NO_3)_3$

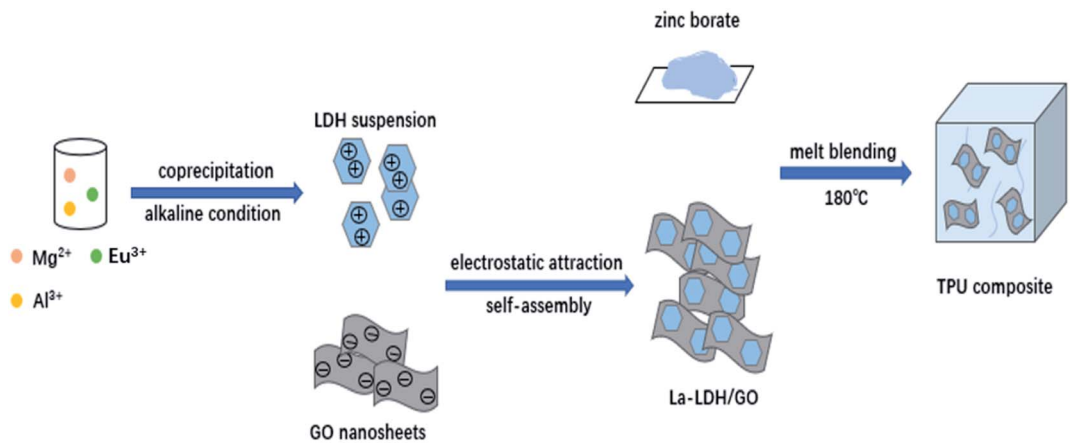

Fig. 1 Schematic diagram of material preparation process.

Table 1 Components of TPU composites

Sample code	TPU (wt%)	ZB (wt%)	0.05Eu-LDHs (wt%)	Eu-LDHs/GO (wt%)
TPU	100	0	0	0
TPZ1	90	10	0	0
TPZ2	90	8	2	0
TPZ3	90	8	0	2

and $Eu(NO_3)_3$ into a three-mouth flask, control the total molar amount of La^{3+} and Al^{3+} constant to 0.012 mol, the molar ratio of La^{3+}/Al^{3+} to 0.05, and then add 3% GO dispersion. Add 5 wt% dilute ammonia solution to the mixed solution drop by drop at 65 °C, adjust the pH value to 10 and continue stirring for 30 min. After stirring, the suspension was transferred to a Teflon reactor for reaction at 130 °C for 12 h. After the reaction, the product was cooled to room temperature, filtered and washed with deionized water until neutral. After drying at 60 °C for 12 h, the sample was ground to obtain Eu-LDHs/GO hybrid material.

2.4 Synthesis of TPU composites

TPU composites were prepared by melt blending method. Approximately 50 g of pure TPU is put into an internal mixer at 180 °C and stirred for 3 min at a stirring speed of 30 rpm. Then, a certain amount of Eu-LDHs/GO was mixed with zinc borate at different proportions and added it into. The mixture was stirred continuously for 10 min at the 180 °C. Finally, the TPU composite containing flame retardant was pressed at 180 °C and 10 MPa for 10 min to form a sheet of 10 cm × 10 cm × 0.3 cm. The components of all TPU composites are shown in Table 1.

2.5 Characterization

X-ray diffraction (XRD) test was performed by Rigaku X-ray diffractometer (Japan), which uses Cu-Kα tubes and Ni filters ($\lambda = 0.1542$ nm). Fourier transform infrared spectroscopy (FTIR) were recorded on a Nicolet 6700 FTIR spectrometer (USA) with a wavelength range of 400–4000 cm^{-1}. Scanning Electron Microscope (SEM)-Energy Dispersive Spectrum (EDS) analysis and test by a Japanese JMS-6700 apparatus with an acceleration voltage of 8 kV. The transmission electron microscope test was performed by Japan JEM-2100 plus instrument under the condition of 200 kV acceleration voltage. Cone calorimeter (CCT) is tested by Chinese JCZ-2 cone calorimeter, the test standard is ISO 5660 and the thermal radiation power is 50 kW km^{-2}. The size of the sample tested by the cone calorimeter was 10 cm × 10 cm × 0.3 cm. Thermalgravimetric analysis (TGA) was carried out on a DT-50 instrument (France). The samples were heated from 40 °C to 800 °C. The heating rates were set as 20 °C min^{-1} (nitrogen atmosphere, flow rate of 20 mL min^{-1}).

3. Results and discussion

3.1 Characterization of as-prepared samples

XRD is usually used to characterize the crystal structure of materials. Fig. 2 shows the XRD spectra of Eu-LDHs materials

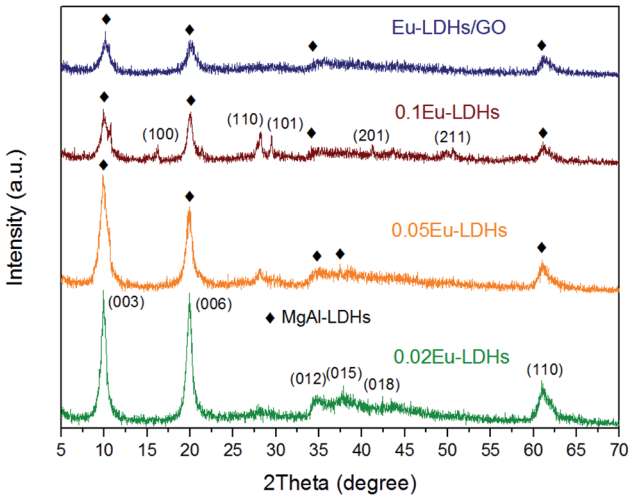

Fig. 2 XRD spectra of 0.02Eu-LDHs, 0.05Eu-LDHs, 0.1Eu-LDHs and Eu-LDHs/GO.

with different Eu^{3+}/Al^{3+} molar ratios and Eu-LDHs/GO hybrid materials. As can be seen from the figure, for all Eu-LDHs, the diffraction angles of (003), (006) and (110) crystal planes corresponding to the diffraction peaks have a good ordered multiple relationship, indicating the layered structure of Eu-LDHs. The spectrum of 0.02 Eu-LDHs showed diffraction peaks at the diffraction angles of 9.9°, 20.0°, 34.8°, 37.9°, 42.4° and 61.2°, respectively, corresponding to the (003), (006), (012), (015), (018) and (110) characteristic crystal planes of LDHs.[19] The intensity of the three diffraction peaks of 0.02Eu-LDHs between 30° and 50° was reduced, and the peak shape was no longer sharp. This was due to the decrease of crystallinity of LDHs caused by the introduction of Eu^{3+}. With the increase of Eu^{3+} concentration, for 0.05Eu-LDHs, the intensity of each peak in the spectrum further decreased, the diffraction peak corresponding to the (018) crystal plane disappeared, and the peak pattern of the diffraction peak corresponding to the (012) and (015) crystal planes became blunter.

Through XRD test, the structural parameters of Eu-LDHS were obtained as shown in Table 2. In the table, cell parameter (d) is the interlamellar distance of LDH, (a) is the distance between metal cations in LDHS lamellar plate, and cell parameter (c) is the cell thickness of LDHs.[20] As can be seen from the table, the (a) value of La-LDHs decreases while the c value increases compared with that of MgAl-LDHs. This is mainly because the ion radius of Eu^{3+} is larger than that of Al^{3+}. When Eu^{3+} replaces Al^{3+} and enters LDH lamina, it will destroy

Table 2 Indexing of XRD spectra for 0.02Eu-LDHs, 0.05Eu-LDHs and 0.1Eu-LDHs

Sample code	d_{003} (nm)	d_{006} (nm)	d_{110} (nm)	a (nm)	c (nm)
0.02Eu-LDHs	0.8893	0.4445	0.1513	0.3026	2.6675
0.05Eu-LDHs	0.8982	0.4441	0.1515	0.3030	2.6796
0.1Eu-LDHs	0.8908	0.4428	0.1517	0.3034	2.6646

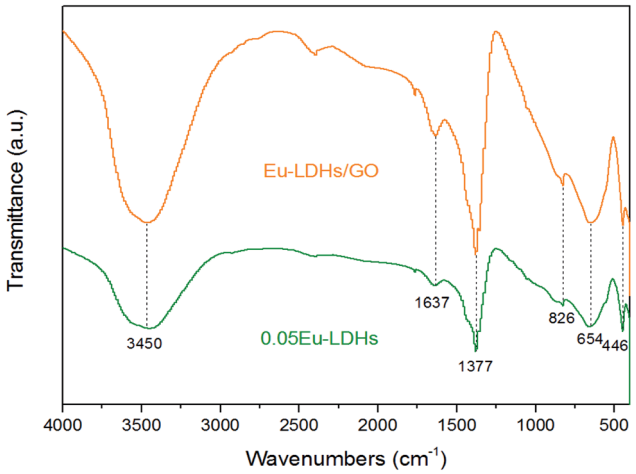

Fig. 3 FTIR spectra of 0.05Eu-LDHs and Eu-LDHs/GO.

the original octahedral structure of MgAl-LDHs. At the same time, the destruction of octahedral structure weakens the electrostatic force between the laminates, resulting in the increase of cell thickness. It is worth noting that when the mole ratio of Eu^{3+}/Al^{3+} is 0.1, the characteristic peak of LDHs in the 0.1Eu-LDHs spectrum further decreases. At this time, the diffraction peaks corresponding to the (015) and (018) crystal planes disappear, but appear at the diffraction angles of 16.3°, 28.2°, 29.5°, 41.2° and 50.7°. These diffraction peaks correspond to the characteristic crystal faces of (100), (110), (101), (201), and (211) of $Eu(OH)_3$ respectively. This is also due to the high concentration of Eu, the excess Eu can not form MO_6 octahedral structure, thus generating $Eu(OH)_3$.[21] Therefore, based on the XRD analysis results of 0.1 Eu-LDHs, the Eu-LDHs/GO hybrid material was also prepared with 0.05Eu-LDHs without hetero phase. From the XRD spectra of Eu-LDHs/GO hybrid materials, as can be seen that the characteristic peaks of Eu-LDHs/GO hybrid materials are basically the same as the characteristic peaks of 0.05 Eu-LDHs, but there is no GO characteristic peak.

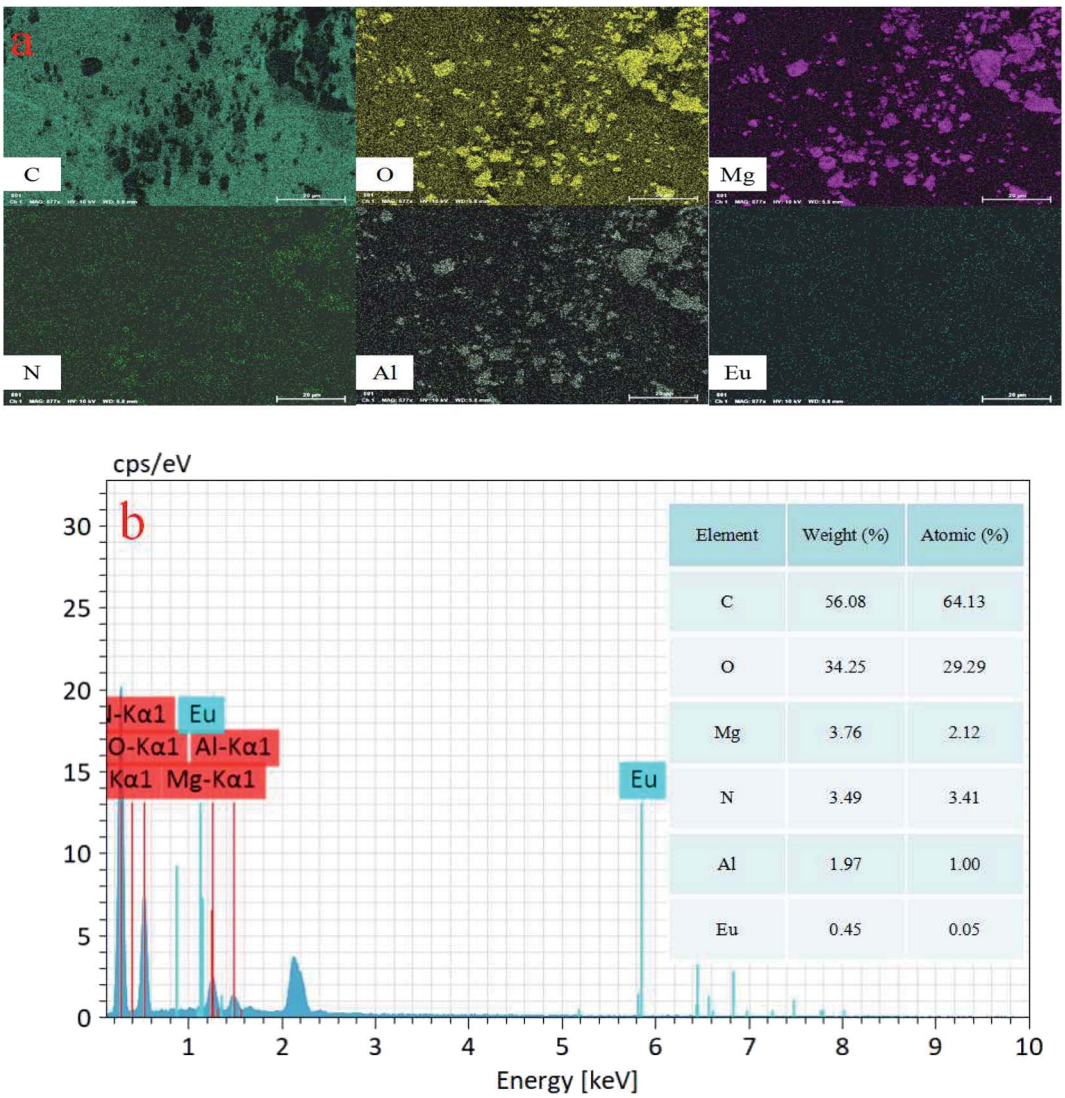

Fig. 4 EDS spectrum (a) and plan scan image (b) of Eu-LDHs/GO.

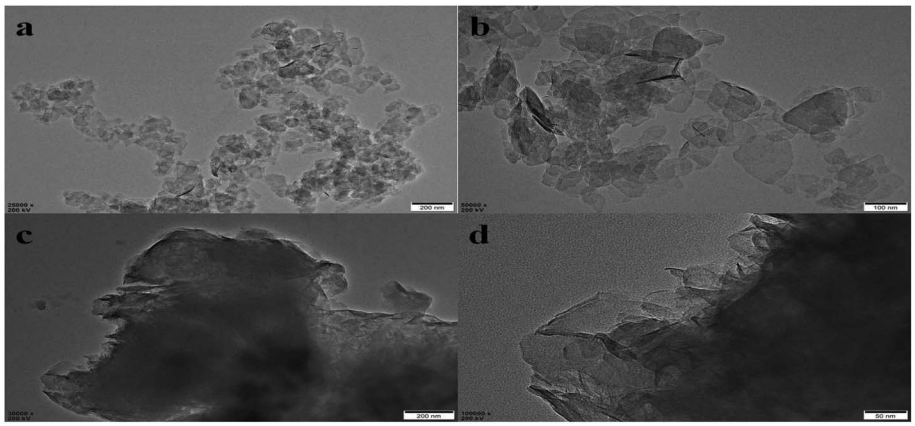

Fig. 5 TEM images of 0.05Eu-LDHs (a and b) and Eu-LDHs/GO (c and d).

This was because Eu-LDHs coated GO by electrostatic force, indicating that 0.05Eu-LDHs nanosheets were successfully loaded onto GO layers.

The FTIR test can obtain the spectra of the chemical bonds and the absorption peaks of functional groups of the material, determine the chemical composition of the material. The FTIR spectra of 0.05Eu-LDHs and Eu-LDHs/GO hybrid materials are shown in Fig. 3. As can see from the picture, the absorption peaks of 0.05 Eu-LDHs at wave numbers 3450 cm^{-1} and 1637 cm^{-1} respectively correspond to the stretching vibration of O–H and the deformation vibration of H_2O. The characteristic peaks at 1377 cm^{-1} and 826 cm^{-1} correspond to the vibration of NO_3^- (ν_3 and ν_2) between the layers of LDHs.[22] Compared with the spectrograms of 0.05Eu-LDHs and MgAl-LDH, the occurrence locations of the characteristic absorption peaks of the both were basically the same. However, the absorption peaks of Al–O in the spectrograms of 0.05Eu-LDHs also shifted from 666 cm^{-1} to 654 cm^{-1}, and the absorption peaks at 555 cm^{-1} disappeared, indicating that Eu^{3+} destroyed the lattice structure of MgAl-LDH after replacing Al^{3+}.[23,24] In addition, the FTIR spectra of 0.05Eu-LDHs and Eu-LDHs/GO hybrid materials basically coincide, and the intensity of each absorption peak is slightly changed without the occurrence of GO absorption peak, which is caused by the successful loading of 0.05Eu-LDHs onto the GO sheet layer, which is consistent with the results of XRD analysis.[25]

Fig. 4 shows the EDS spectrum and planar scan of Eu-LDHs/GO hybrid materials. As shown in Fig. 4(a), the main components of Eu-LDHs/GO hybrid materials are C, O, Mg, N, Al and Eu, and the distribution of Mg, Al and Eu elements is relatively uniform, which confirms the successful entry of Eu^{3+} into the MgAl-LDHs layer. At the same time, it can be observed from Fig. 4(b) that the content of element C in Eu-LDs/GO hybrid material is the highest, which proves the existence of GO. Moreover, the molar ratio of $Mg^{2+}/Al^{3+}/Eu^{3+}$ is 2.1/1/0.05, which is basically consistent with the calculated results during the preparation of the material.

Fig. 5 shows the TEM images of 0.05Eu-LDHs and Eu-LDHs/GO hybrid materials. As can be seen from Fig. 5(a and c), 0.05Eu-LDHs has an obvious layered structure with a particle size of about 100 nm. Due to the partial replacement of Al^{3+} in the MgAl-LDHs lamellae by Eu^{3+}, the appearance of 0.05Eu-LDHs is irregular. The Eu-LDHs/GO hybrid materials is shown in Fig. 5(c and d), many 0.05Eu-LDHs tablets appeared on the

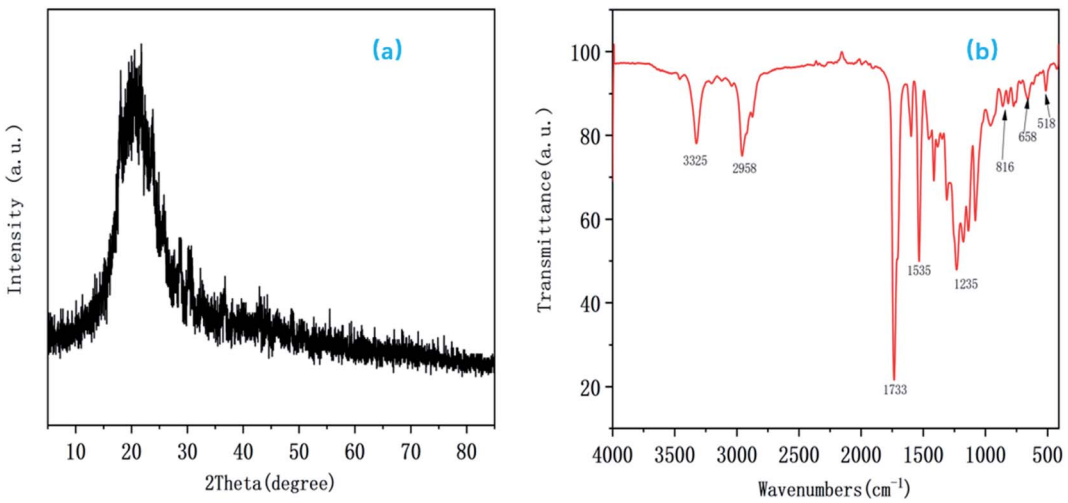

Fig. 6 XRD patterns of TPU composites (a); FTIR spectrum of TPU composites (b).

Table 3 Cone calorimeter data of TPU composites

Sample code	PHRR, kW m^{-2}	THR, MJ m^{-2}	AvHRR, kW m^{-2}	PSPR, m^2 s^{-1}	TSP, m^2	AvSEA, m^2 kg^{-1}	AvCOY, kg kg^{-1}
TPU	1103	139.1	261.2	0.100	13.22	159.6	0.011
TPZ1	441	123.1	158.4	0.058	8.96	73.4	0.006
TPZ2	430	119.8	146.2	0.042	8.92	61.8	0.004
TPZ3	379	116.6	145.4	0.039	8.32	61.5	0.002

GO chip layer, effectively inhibiting the aggregation of GO, so the overlap area was significantly reduced.[26] The results of XRD, FTIR, EDS and TEM all proved the successful preparation of Eu-LDHs/GO hybrid materials.

Fig. 6(a) shows the XRD pattern of TPU composites. It can be seen that with the addition of ZB and Eu-LDH/GO, the peak shape of TPU composites is still consistent with that of pure TPU. This indicates that the basic structure of TPU has not been changed by the addition of the flame retardant, and the flame retardant is uniformly dispersed in the TPU matrix.[27] Fig. 6(b) shows the FTIR spectrum of TPU composites. In the figure, the absorption peak at 3325 cm^{-1} is $-NH_2$ telescopic vibration, the absorption peak at 2958 cm^{-1} is –C–N vibration absorption, and the absorption peak at 1733 cm^{-1} is –C═O– vibration absorption. The 816 cm^{-1} is N–O vibration absorption peak, while the characteristic peaks of amide II band (V (C–N) + σ(N–H)) and amide III band (V (C–N) + σ(N–H)) appear near 1250 cm^{-1} and 1530 cm^{-1}, which are the characteristic peaks of polyether type TPU. The characteristic peaks at 518 cm^{-1} and 658 cm^{-1} correspond to M–O stretching vibration on Eu-LDH laminates.[28] The above analysis shows that the TPU composite prepared by melt blending method still retains the original structure of TPU.

3.2 Flame retardancy of TPU composites

The parameters related to flame retardant and smoke suppression of the composite can be measured by cone calorimeter.[29,30] The data analyzed by cone calorimeter (CCT) are shown in Table 3, and the heat release rate (HRR) curve of TPU composites is shown in Fig. 7. As can be seen from the curve, the heat of pure TPU increases sharply after ignition. Since TPU is basically non-carbonized in the combustion process, and it is also unstable even if it can form a carbon layer. So it cannot protect the TPU matrix, the HRR curve drops rapidly after reaching the peak (1103 kW m^{-2}), and a shoulder peak appears. For TPZ1 with an added ZB of 10 wt%, the peak heat release rate (PHRR) is 441 kW m^{-2}, which is 60.0% lower than pure TPU. This benefits from the good flame retardant effect of ZB on TPU. On the one hand, ZB thermal decomposition and dehydration will absorb heat and dilute the concentration of combustible gas, so that it does not reach the lower limit of combustion. On the other hand, ZB can promote TPU to form a protective carbon layer after dehydration, thus effectively inhibiting the oxidation and thermal decomposition of TPU.[31] When the ZB of 2 wt% in TPU was replaced by 0.05Eu-LDHs and Eu-LDHs/GO hybrid materials, the PHRR value of TPZ2 and TPZ3 decreased further compared with TPZ1, and the PHRR value of TPZ3 was the lowest, decreasing by 65.6% compared with pure TPU. This shows that ZB combined with Eu-LDHs/GO hybrid material has a good synergistic effect on flame retardant. At the same time, by comparing the three TPU composites containing ZB, it can be found that their HRR curves have similar trends and are also thermally thick carbonized samples. After reaching the peak, they all decline slowly and tend to be stable, which is the effect of protective carbon layer. In addition, combined with the data in Table 3, average heat release rate (AvHRR) of TPZ1, TPZ2 and TPZ3 decreased to 158.4 kW m^{-2}, 146.2 kW m^{-2} and 145.4 kW m^{-2}, which were significantly lower than pure TPU (261.1 kW m^{-2}).

Fig. 8 shows the total heat release (THR) curve of TPU composites. As can be seen from the figure that the slope of

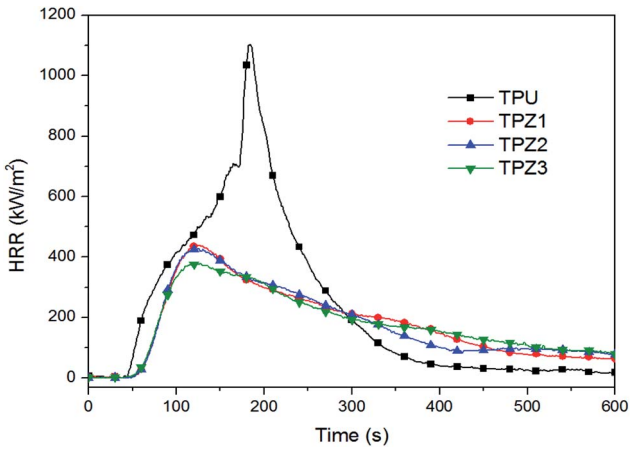

Fig. 7 HRR curves of TPU composites.

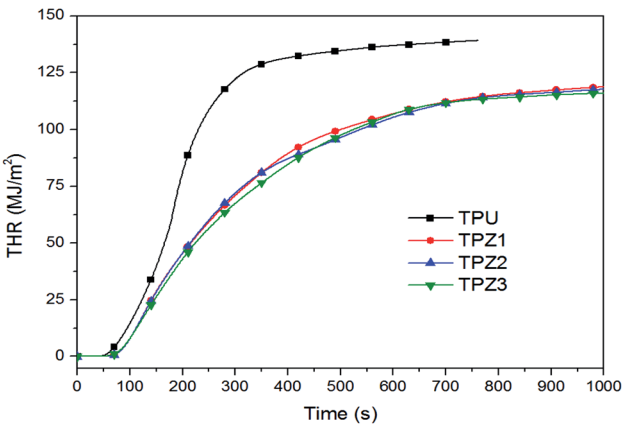

Fig. 8 THR curves of TPU composites.

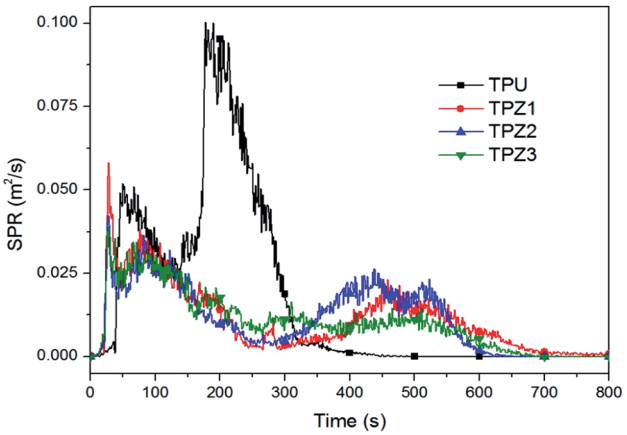

Fig. 9 SPR curves of TPU composites.

THR curve of all samples is basically the same in the stage of 100–150 s, but the three TPU materials containing ZB start to release heat later than pure TPU, which is consistent with the HRR analysis results. Immediately after at 150 s, the THR curve of pure TPU rises rapidly, and an inflection point occurs at about 350 s. After that, the curve flattens out with a THR value of 139.1 MJ m^{-2}, which also indicates that TPU combustion will release a large amount of heat rapidly. For TPZ1, TPZ2 and TPZ3, THR curves of the three are similar in trend. The slope decreases and gradually becomes stable at 150 s without obvious inflection point, the THR values are 123.1 MJ m^{-2}, 119.8 MJ m^{-2} and 116.6 MJ m^{-2}, respectively. In the combustion process, ZB has a good performance in reducing the heat of TPU, which is not only related to heat absorption and carbonization by thermal decomposition, but also ZnO and $Zn(OH)_2$ generated by ZB decomposition will enter the gas phase in the form of gas and dilute the concentration of combustible gas.[32] Therefore, ZB has a more significant gas-phase flame retardant effect. The THR value of TPZ3 was the lowest among all the samples, and the THR value of TPZ3 was reduced by 16.2% compared with pure TPU. In addition to 0.05Eu-LDHs and GO heat absorption and carbonization, ZB and Eu-LDHs/GO hybrid materials showed better synergistic flame retardant effect than Eu-LDHs/GO due to good gas phase dilution and solid phase overlay of ZB.

3.3 Smoke suppression of TPU composites

In addition to the heat release during combustion, the fire risk of composites also depends on the amount of smoke produced during combustion.[33] Through CCT test, can also get the smoke parameters of the composite combustion. The smoke production rate (SPR) curve of TPU composite materials shows in Fig. 9. As can see from the picture, the SPR curve of pure TPU appears a small peak value of 0.052 m^2 s^{-1} at about 50 s. This phase belongs to the smoke generation stage of TPU flameless combustion, indicating that TPU is easy to smolder. Later, when flashover occurs in TPU, the smoke diffuses rapidly and the SPR curve rises rapidly, reaching the smoke production rate (PSPR) value of 0.100 m^2 s^{-1} at about 200 s. When adding ZB to TPU, the TPZ1 SPR curve arrive PSPR value (0.058 m^2 s^{-1}) quickly. However, it does not have the same maximum peak as pure TPU, but quickly reaches a small peak (0.038 m^2 s^{-1}) at about 100 s. Following, the SPR curve gradually declining. On the one hand, this is because the ZB can inhibit the TPU smoldering and makes the TPU in advance into the flaming stage. On the other hand, it also reduced the smoke particles produce no flame combustion. The result is consistent with the HRR and THR. The ZB has good smoke suppression performance on TPU. Firstly, the flame-retardant effect of ZB inhibits the further combustion of TPU substrate, thus fundamentally reducing the generation of smoke. Secondly, water vapor generated by thermal decomposition of ZB can condensate on smoke particles, and smoke particles collide with each other and condensate. Thus accelerating the sedimentation, making smoke particles enter into the condensed phase from the gas phase, effectively reducing the generation and release of smoke.[34] When ZB was compounded with 0.05Eu-LDHs, the PSPR value of TPZ2 further decreased to 0.042 m^2 s^{-1}, indicating that the water vapor released by the thermal decomposition of 0.05Eu-LDHs and the alkaline lamellae played an inhibitory effect on smoke. Meanwhile, among all the samples, TPZ3 had the lowest PSPR value of 0.039 m^2 s^{-1}, which was 61% lower than pure TPU. ZB and 0.05Eu-LDHs combined with the physical barrier effect of GO to promote carbon formation and could better protect the TPU matrix and suppress the release of flue gas. We need to nothing that for all TPU composite material with ZB added, the SPR curve there was a peak in the 500 s. This is because ZB can promote the formation of porous carbon layer in TPU during combustion. When burning into the later period, with the accumulation of heat, the smoke particles can are slowly released on the surface of the carbon layer by the action of many holes in the carbon layer. Therefore, the SPR curve shows as broad peak, but the peak value of TPZ3, TPZ1 and TPZ2 is lower, it more confirmed ZB and Eu-LDHs/GO hybrid materials better synergistic effect of smoke suppression.

Fig. 10 shows the total smoke production (TSP) curve of TPU composite. It can be seen from the figure that the slope of TSP curve of pure TPU increases significantly and turns to inflection

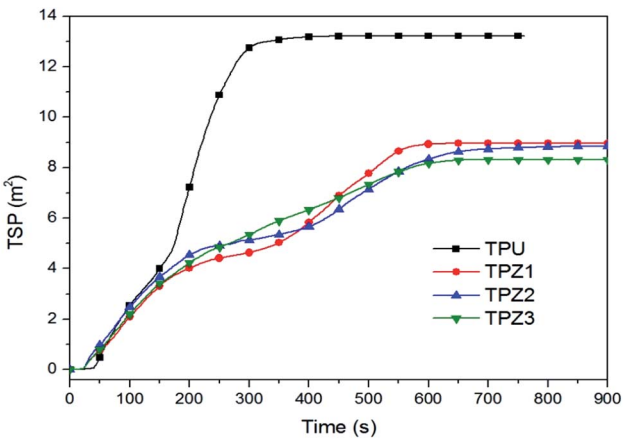

Fig. 10 TSP curves of TPU composites.

point when it is about 200 s, which is corresponding to the SPR curve. Pure TPU reaches the PSPR value at this point, and the smoke output increases significantly, and the final TSP value is 13.22 m^2. For TPZ1 containing only ZB, the TSP curve also appears an inflection point at 200 s, but the slope decreases. It indicates that the presence of ZB can not only inhibit smolder of TPU, but also shorten the flame burning time of TPU and reduce the smoke generation. At about 400 s, the TSP curve slope of TPZ1 increases and another inflection point appears, which is consistent with the SPR curve of starting to appear at about 400 s. From TPZ1 to TPZ3, this inflection point gradually disappears. The TSP curve of TPZ3 has no inflection point and basically flattens out gradually. Meanwhile, the TSP values of TPZ1, TPZ2 and TPZ3 were 8.96 m^2, 8.92 m^2 and 8.32 m^2, respectively. In contrast with pure TPU, the TSP value of TPZ3 was the lowest, with a decrease of 37.1%. The above results indicate that ZB and Eu-LDHs/GO hybrid materials have a good synergistic effect on TPU and greatly reduce the smoke generation during combustion. In addition, combined with the data in Table 2, average specific extinction area (AvSEA) values of TPZ1, TPZ2 and TPZ3 are 73.4 $m^2\ kg^{-1}$, 61.8 $m^2\ kg^{-1}$ and 61.5 $m^2\ kg^{-1}$, respectively, which are greatly reduced compared with pure TPU (159.6 $m^2\ kg^{-1}$). Because the smoke contains smoke particles, which can scatter and absorb light. As a result, this will reduce the visibility of the fire site, affecting rescue and evacuation efforts. AvSEA value of TPZ3 significantly decreases, which proves that ZB and Eu-LDHs/GO hybrid materials can better reduce the light attenuation of smoke. Meanwhile, compared with pure TPU, the average CO yield (AvCOY) of the three ZB-containing TPU composites also decreased further, with the decrease of TPZ3 up to 81.1%. This result is attributed to the large specific surface area of GO, which can effectively adsorb CO and other toxic gases.[35] Therefore, the ZB and Eu-LDHs/GO hybrid material in the combustion process of TPU can not only assist smoke suppression, can also assist effect attenuated.

3.4 Thermal stability of TPU composites

Mass loss is the percentage of the residual mass and the initial mass of the sample after combustion. By analyzing the mass loss of the sample, the flame retardant mechanism of the solidified phase can be studied to a certain extent. Fig. 11 shows the thermogravimetry (TG) and derivative thermogravimetry (DTG) curves of TPU composites under N_2 protective atmosphere. As can be seen from the figure, the mass loss curve of pure TPU begins to decline rapidly at 300 °C, and another inflection point appears at 400 °C. As the combustion ends, the curve flattens out due to the lack of a carbon layer. TPZ1, TPZ2 and TPZ3 have similar mass loss curves, but TPZ1, TPZ2 and TPZ3 all start weightlessness earlier than pure TPU, and the end time of weightlessness is earlier. These results indicate that ZB, 0.05Eu-LDHs and Eu-LDHs/GO hybrid materials decompose at lower temperature, thus improving the thermal stability of TPU matrix and reducing the heat release, which is consistent with the HRR analysis results. From the of mass loss rate analysis, the DTG curve of pure TPU has two separation peaks. The first

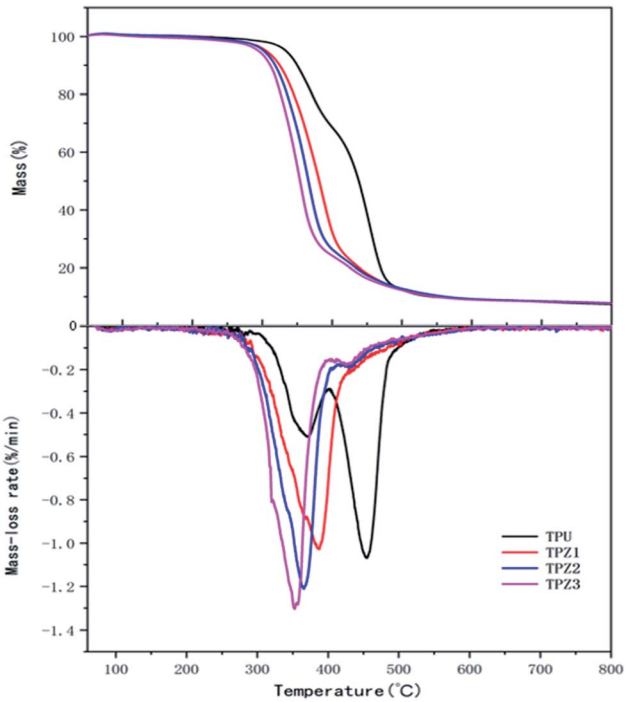

Fig. 11 TG and DTG curves of TPU composites.

peak is mainly attributed to the removal of CO_2, and the second peak is mainly attributed to the dehydration and oxidation reaction.[36] There is only one peak of TPZ1, TPZ2 and TPZ3 due to the carbonization process during combustion, which further confirms that pure TPU is non-carbonization type sample. TPZ1, TPZ2 and TPZ3 belong to thermogenic carbonaceous type, and TPZ3 formed carbonaceous layer earlier than TPZ2 and TPZ1. First, it is because ZB reduces the heat release in the combustion process and delays the further combustion of the TPU matrix. Secondly, after ZB is melted at high temperature, vitrified coating material will be formed to cover the TPU matrix and form a porous carbon layer, which is conducive to blocking heat transfer and prevent O_2 from diffusing into the TPU. When ZB is combined with Eu-LDHs and Eu-LDHs/GO mixed materials, the carbon formation effect of TPZ2 and TPZ3 is more obvious, and the thermal stability is better. Similar to thermoplastic polyurethane, when 7.5% ZB flame retardant is added to waterborne TU, the composite material begins to lose weight at 90 °C, and reaches the maximum weight loss rate of 20 mass% min^{-1} at 400 °C.[37] Therefore, the thermal stability of the TPU composite is obviously better than that of the water-based PU.

3.5 Char residue test of TPU composite material

In order to further explore the mechanism of the cohesion of ZB and Eu-LDHs/GO hybrid materials on TPU and the synergistic flame retardancy and smoke suppression, we also need to use SEM, XRD and other methods to analyze the morphology and structure of the carbon slag after CCT testing.[38] Fig. 12 displays the SEM diagram of TPU composite carbon slag after CCT. We can be learn from the figure that when pure TPU burns out, the

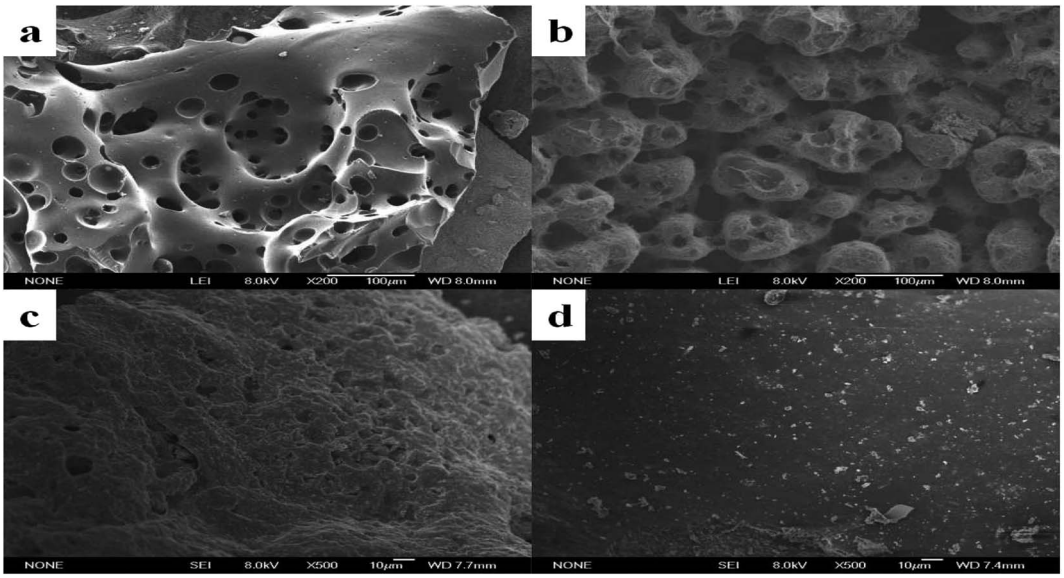

Fig. 12 SEM images of carbon residues of TPU (a), TPZ1 (b), TPZ2 (c) and TPZ3 (d).

carbon slag formed has many holes on the surface, which are loose and fragile. The diameter of the holes is about 30–50 μm, which also indicates that TPU is basically carbonless during combustion. Since TPZ1 only contains ZB, a large number of small holes still appear on the surface of the carbon residue, the diameter of which is about 10–20 μ. It unlike pure TPU, pure TPU basic throughout the carbon residue of the holes for carbon residue and TPZ1 carbon slag hole is mainly on the surface in the form of depression, and the diameter of the pure TPU is much smaller. In some extent, these holes can inhibit the TPU flue gas and heat transfer in the combustion process. For TPZ2, when 0.05Eu-LDHs was added to TPU, the catalytic carbonization of 0.05 Eu-LDHs significantly reduced the pores on the surface of carbon residue, but the surface was still rough. However, for TPZ3 compound of adding ZB and Eu-LDHs/GO, the surface of carbon residue basically has no pores and becomes smooth and dense. This is mainly due to the combination of physical barrier of GO, so the presence of Eu-LDHs/GO hybrid material can stabilize the porous carbon layer generated under the action of ZB.

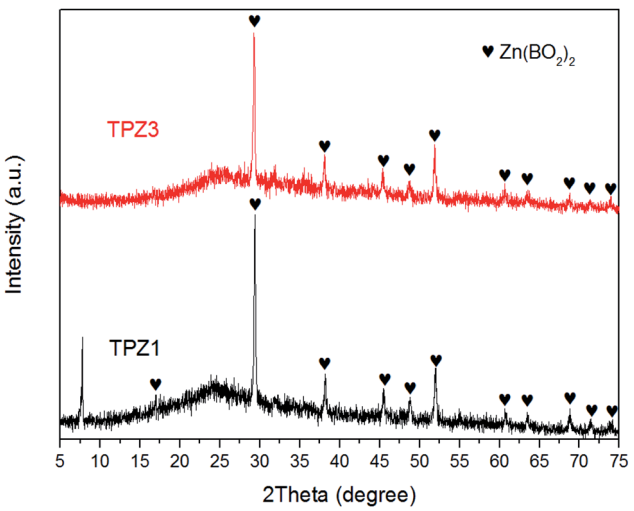

Fig. 13 XRD patterns of char residues of TPZ1 and TPZ3.

Fig. 13 shows the XRD patterns of TPZ1 and TPZ3 carbon residues. As shown in the figure, diffraction peaks of TPZ1 carbon slag at diffraction angles of 17.0°, 29.4°, 38.2°, 45.5°, 48.8°, 52.0°, 60.7°, 68.8°, 71.4° and 74.1° correspond to (110), (211), (310), (321), (400), (330), (422), (521), (440) and (530) characteristic crystal surfaces of $Zn(BO_2)_2$ (JCPDS card no. 39-1126) respectively. Combined with SEM analysis results, it shows that after ZB is melted at high temperature, most elements of B and Zn will still remain on TPZ1 carbon slag, thus forming glassy coverings. At the same time, the spectrum of TPZ1 carbon slag shows the diffraction peak of symmetrical vibration of graphite microcrystalline near the diffraction angle of 25°, which proves that the carbon slag of TPZ1 also contains graphitized structure. For TPZ3 carbon slag, diffraction peaks of $Zn(BO_2)_2$ and graphite microcrystals also appeared in the spectrogram. Compared with TPZ1 carbon slag, the intensity was basically unchanged, and the impurity peaks at the diffraction angle of 7.8° disappeared, which further indicated that the co-effect of ZB and Eu-LDHs/GO hybrid materials could not only change the morphology of carbon layer, but also improve the strength of carbon layer.[39] The stronger the carbon layer, the more complete the surface and the stronger the ability to protect the TPU substrate from further erosion by flame.

4. Conclusions

In summary, this article combines the advantages of rare earth europium, hydrotalcite, graphene oxide and zinc borate, and uses co-precipitation and hydrothermal methods to synthesize Eu-LDHs/GO hybrid materials. The next, it was characterized by XRD, FTIR, EDS and TEM, indicating the successful synthesis of

the material. After that, we mixed the Eu-LDHs/GO hybrid material with zinc borate in a ratio of 1 : 4, and added it to the TPU by melt blending. Finally, the fire safety performance are tested. The results show that, compared with TPU1 and TPU2, the fire safety of TPU3 is more significantly improved, which is attributed to the good synergistic flame retardant effect of Eu-LDHs/GO hybrid material and ZB in TPU. The PHRR, THR, PSPR and TSP values of TPZ3 decreased by 65.6%, 16.2%, 61% and 37.1% respectively compared to pure TPU. In addition, the carbon formation rate after TPZ3 combustion is also significantly increased. The results of carbon residue analysis show that the addition of europium in hydrotalcite can improve the carbon formation rate in the matrix, and the synergistic effect of Eu-LDHs/Go and ZB can promote the stable porous carbon layer in the matrix after combustion. Therefore, the resistance mechanism of the composite material is as follows. The first is that the water vapor from the decomposition of hydrotalcite in the matrix combustion can dilute the combustible gas. Secondly, graphene oxide (GO) can act as a sheet barrier during matrix combustion, isolating the release of combustible gas and heat transfer. Finally, Eu-LDHs/GO and ZB cooperate to form a stable porous carbon layer during matrix combustion, which can not only prevent heat transfer, but also absorb the generated smoke.

Conflicts of interest

There are no conflicts to declare.

Acknowledgements

The authors gratefully acknowledge the National Natural Science Foundation of China (No. 51572138), the Key R&D Project of Shandong Province (No. 2019GSF109001, 2019CSF109080), the Shandong Provincial Natural Science Foundation, China (No. ZR2018BB072), the Original Innovation Project of Qingdao City (No. 19-6-2-23-cg), the Foundation of State Key Laboratory of High-Efficiency Utilization of Coal and Green Chemical Engineering (No. 2018-K09 and 2018-K43), Key Laboratory of Coastal Environmental Processes and Ecological Remediation, YICCAS (No. 2018KFJJ02) and Opening Project of Shandong Eco chemical Engineering Collaborative Innovation Center (No. XTCXQN02).

References

1 S. Aleksandra, M. Z. Elke, G. Michael, *et al.*, Rapid mass calorimeter as a high-throughput screening method for the development of flame-retarded TPU, *Polym. Degrad. Stab.*, 2018, **156**, 43–58.

2 X. Chen, W. Wang and C. Jiao, A recycled environmental friendly flame retardant by modifying para-aramid fiber with phosphorus acid for thermoplastic polyurethane elastomer, *J. Hazard. Mater.*, 2017, **331**, 257–264.

3 A. B. Morgan and J. W. Gilman, An overview of flame retardancy of polymeric materials: application, technology, and future directions, *Fire Mater.*, 2013, **37**(4), 259–279.

4 W. Wei, C. Deng, S. Huang, *et al.*, Nickel-Schiff base decorated graphene for simultaneously enhancing the electroconductivity, fire resistance, and mechanical properties of a polyurethane elastomer, *J. Mater. Chem. A*, 2018, **6**(18), 8643–8654.

5 S. Xu, M. Zhang, S. Y. Li, *et al.*, Intercalation of a novel containing nitrogen and sulfur anion into hydrotalcite and its highly efficient flame retardant performance for polypropylene, *Appl. Clay Sci.*, 2020, **191**, 150–165.

6 Y. Liu, Y. Gao, Q. Wang, *et al.*, Synergistic effect of layered double hydroxides with other flame retardant additives for polymer nanocomposites: a critical review, *Dalton Trans.*, 2018, **47**(42), 14827–14840.

7 R. J. Wen, Z. H. Yang, H. Y. Chen, *et al.*, Zn-Al-La hydrotalcite-like compounds as heating stabilizer in PVC resin, *J. Rare Earths*, 2012, **30**(9), 895–902.

8 X. Li, Y. Tao, F. Li and M. Huang, Efficient Preparation and Characterization of Functional Graphene with Versatile Applicability, *J. Harbin Inst. Technol.*, 2016, **23**(3), 1–29.

9 Y.-B. Xie, M.-R. Huang and X.-G. Li, Review: Layer-Number Controllable Preparation of High-Quality Graphene for Wide Applications, *J. Harbin Inst. Technol.*, 2020, **27**(3), 136–157.

10 J. Y. Wang, X. Y. Mei, L. Huang, *et al.*, Synthesis of layered double hydroxides/graphene oxide nanocomposite as a novel high-temperature CO_2 adsorbent, *J. Energy Chem.*, 2015, **24**(2), 127–137.

11 N. S. Ahmed, R. Menzel, Y. F. Wang, *et al.*, Graphene-oxide-supported CuAl and CoAl layer double hydroxides as enhanced catalysts for carbon-carbon coupling via Ullmann reaction, *J. Solid State Chem.*, 2017, **246**, 130–137.

12 N. N. Hong, L. Song, B. B. Wang, *et al.*, Co-precipitation synthesis of reduced graphene oxide/NiAl-layered double hydroxide hybrid and its application in flame retarding poly(methyl methacrylate), *Mater. Res. Bull.*, 2014, **49**, 657–664.

13 L. H. Ai, L. Yang, J. F. Hu, *et al.*, Synergistic Flame Retardant Effect of Organic Boron Flame Retardant and Aluminum Hydroxide on Polyethylene, *Fibers Polym.*, 2021, **3**, 1–12.

14 N. Wang, M. H. Zhou, J. Zhang, *et al.*, Modified boron nitride as an efficient synergist to flame retardant natural rubber: preparation and properties, *Polym. Adv. Technol.*, 2020, **31**(9), 1887–1895.

15 B. Yildiz, M. Ö. Seydibeyoğlu and F. S. Güner, Polyurethane-zinc borate composites with high oxidative stability and flame retardancy, *Polym. Degrad. Stab.*, 2009, **94**(7), 1072–1075.

16 S. Yang, Y. Liu, *et al.*, Synergism of poly siloxane and zinc borate flame retardant polycarbonate, *Polym. Degrad. Stab.*, 2013, **98**(12), 2795–2800.

17 J. S. Sun, Q. Ge, J. Yang, *et al.*, Synthesis of zinc borate and its application in flame retardant polyolefin, *Plast. Addit.*, 2018, **4**, 6–12.

18 S. Park, D. Piner, *et al.*, Aqueous suspension and characterization of chemically modified graphene sheets, *Chem. Mater.*, 2008, **20**(21), 6592–6594.

19 S. P. Lonkar, B. Kutlu, A. Leuteritz, *et al.*, Nanohybrids of phenolic antioxidant intercalated into MgAl-layered double hydroxide clay, *Appl. Clay Sci.*, 2013, **71**, 8–14.

20 L. Mao. *Design and synthesis of hydrotalcite containing rare earth elements and properties of polybutene succinate expansion flame retardant system*, Hunan University of Technology, 2014.

21 F. H. Geng, Y. Xin, N. Matsushita, *et al.*, New layered rare-earth hydroxides with anion-exchange properties, *Chem.–Eur. J.*, 2008, **14**(30), 9255–9260.

22 Y. Q. Han, T. Q. Wang, X. X. Gao, *et al.*, Preparation of thermally reduced graphene oxide and the influence of its reduction temperature on the thermal, mechanical, flame retardant performances of PS nanocomposites, *Composites, Part A*, 2016, **84**, 336–343.

23 R. Wen, Z. Yang, H. Chen, *et al.*, Zn-Al-La hydrotalcite-like compounds as heating stabilizer in PVC resin, *J. Rare Earths*, 2012, **30**(9), 895–902.

24 S. Yi, Z. H. Yang, S. W. Wang, *et al.*, Effects of MgAlCe-CO_3 layered double hydroxides on the thermal stability of PVC resin, *J. Appl. Polym. Sci.*, 2011, **119**(5), 2620–2626.

25 K. Zhou, Z. Gui, Y. Hu, *et al.*, The influence of cobalt oxide-graphene hybrids on thermal degradation, fire hazards and mechanical properties of thermoplastic polyurethane composites, *Composites, Part A*, 2016, **88**, 10–18.

26 Y. T. Pan, J. Wan, X. Zhao, C. Li, *et al.*, Interfacial growth of MoF-derived layered double hydroxide nanosheets on graphene slab towards fabrication of multifunctional epoxy nanocomposites, *J. Chem. Eng.*, 2017, **330**, 1222–1231.

27 Y. J. Ma, M. Fang, G. X. Li, *et al.*, Research on Wear Resistance and Thermal Stability of Graphite Reinforced TPU Materials, *Mod. Plast. Process. Appl.*, 201, **33**(01), 1–3.

28 M. Liu, C. Zhang, W. W. Tian, *et al.*, One-step hybridization of graphene nanoribbons with carbon nanotubes and its strong-yet-ductile thermoplastic polyurethane composites, *Polymer*, 2013, **54**, 130.

29 B. Schartel and T. R. Hull, Development of fire-retarded materials-interpretation of cone calorimeter data, *Fire Mater.*, 2007, **31**(5), 327–354.

30 Z. Matusinovic, H. Lu and C. A. Wilkie, The role of dispersion of LDH in fire retardancy: the effect of dispersion on fire retardant properties of polystyrene/Ca-Al layered double hydroxide nanocomposites, *Polym. Degrad. Stab.*, 2012, **97**(9), 1563–1568.

31 T. B. Soo, T. S. Lee, S. C. Boon, *et al.*, Electron beam irradiation of zinc borate flame retardant containing acrylamide-butadiene-styrene (ABS) composites, *J. Polym. Res.*, 2018, **25**(4), 1–16.

32 Y. H. Zheng, Y. M. Tian, H. L. Ma, *et al.*, Synthesis and performance study of zinc borate nano whiskers, *Colloids Surf., A*, 2009, **339**(1), 178–184.

33 L. Liu, X. L. Zhao, C. Y. Ma, *et al.*, Smoke suppression properties of carbon black on flame retardant thermoplastic polyurethane based on ammonium polyphosphate, *J. Therm. Anal. Calorim.*, 2016, **126**(3), 1821–1830.

34 Y. D. Fang, Study on morphology and size change of smoke particles under water mist, *China Eng. Sci.*, 2014, **16**(02), 93–100.

35 S. Wang, R. Gao and K. Zhou, The influence of cerium dioxide functionalized reduced graphene oxide on reducing fire hazards of thermoplastic polyurethane nanocomposites, *J. Colloid Interface Sci.*, 2019, **536**, 127–134.

36 Y. Lv, Y. J. Luo, K. Guo, *et al.*, Study on Thermal decomposition kinetics of GAP energetic thermoplastic Polyurethane, *J. Solid Rocket Technol.*, 2010, **33**(03), 315–318.

37 J. Su, B. Zhou and Y. Shi, Preparation and application of phosphor-nitrogen-boron waterborne polyurethane flame retardant coating, *New Build. Mater.*, 2021, **48**(02), 30–35.

38 J. Yu, Q. Wang, D. O'Hare, *et al.*, Preparation of two-dimensional layered double hydroxide nanosheets and their applications, *Chem. Soc. Rev.*, 2017, **46**(19), 5950–5974.

39 S. Liu, H. Yan, Z. Fang, *et al.*, Effect of graphene nanosheets and layered double hydroxides on the flame retardancy and thermal degradation of epoxy resin, *RSC Adv.*, 2014, **4**(36), 18652–18659.